Vol. 13 (núm. 1) pp. 43-55
Enero-Junio 2022

Ciencia en Desarrollo
Revista de la Facultad de Ciencias
Vicerrectoría en Investigación y Extensión - VIE
Centro de Investigaciones y Extensión de la Facultad de Ciencias - CIEC

https://doi.org/10.19053/01217488.v13.n1.2022.12884

Optical, Electrical, Structural, and Morphological Properties of $KAl_4Si_2O_{12}/Mg_3Si_2O_9/Fe_2O_3$ Clay Mineral from Machado Mountain Region, Tarairá, Colombia

Propiedades ópticas, eléctricas, estructurales y morfológicas de arcilla mineral $KAl_4Si_2O_{12}/Mg_3Si_2O_9/Fe_2O_3$ de la región montañosa de Machado, Tarairá, Colombia

E. F. Galíndez[1,2] J. A. Rojas-Venegas[1], D. Sánchez[1], D. A. Landínez Téllez[3] and J. Roa-Rojas[3]

Abstract

Physical properties of clay minerals are essential in the evaluation for applications and new potential uses of geological materials. This study presents results of optical, electrical, structural, compositional and morphological analysis of Hillite (0.967) / Chlorite (0.013) / Hematite (0.02) clay mineral extracted from the Machado mountain region in the municipality of Tarairá, department of Vaupés, Colombia. The extracted clay was subjected to treatments to separate it from the others geological compounds before the characterization process. The observed platy morphology allowed to perform a size grain analysis which confirmed the clay-extraction. Particles with 0.8- 1.4 μm diameter and two pseudo-modes distribution in the area histogram were found. The bimodal distribution is assumed to be caused due to the differences between periodic ages of formation of the minerals in the extraction region. Structurally, we found a monoclinic structure with residues of triclinic polymorphous and Hexagonal scalenohedral segregated structures. The XRD analysis was based in the EDS measurements, given the stoichiometry of the sample. Also, a big absorption in the optical UV-range with an effective band gap in the clay to 2.852 (8) eV was found. The electrical properties of the clay showed a strong non-linear insulator behavior. Finally, the complete physical properties analysis allowed to introduce this material as an inexpensive, time efficient insulator.

***Keywords*:** Morphology, Clays, Electrical properties, Optical characterization.

Resumen

Las propiedades físicas de los minerales arcillosos son esenciales en la evaluación de aplicaciones y nuevos usos potenciales de materiales geológicos. Este estudio presenta resultados de análisis óptico, eléctrico, estructural, composicional y morfológico de mineral de arcilla Illita (0.967) / Clorita (0.013) / Hematita (0.02) extraído de la región montañosa de Machado en el municipio de Tarairá, departamento de Vaupés, Colombia. La arcilla extraída fue sometida a tratamientos para separarla de los demás compuestos geológicos antes del proceso de caracterización. La morfología laminar observada permitió realizar un análisis de tamaño de grano que confirmó la extracción de arcilla. Se encontraron partículas con un diámetro de 0,8 a 1,4 μm y dos pseudo-modos de distribución en el histograma de áreas. Se supone que la distribución bimodal se debe a las diferencias entre las edades periódicas de formación de los minerales en la región de extracción. Estructuralmente, encontramos una estructura monoclínica con residuos de estructuras segregadas polimorfas triclínicas y escalenoédricas hexagonales. El análisis XRD se basó en las medidas de EDS, dada la estequiometría de la muestra. Además, se encontró una gran absorción en el rango óptico UV con un intervalo de banda efectivo en la arcilla a 2.852 (8) eV. Las propiedades eléctricas de la arcilla mostraron un fuerte comportamiento aislante no lineal. Finalmente, el análisis completo de las propiedades físicas permitió introducir este material como un aislante económico y eficiente en el tiempo.

***Palabras clave*:** Arcillas, Caracterización óptica, Morfología, Propiedades eléctricas.

Recepción: 22-Mayo-2021
Aceptación: 30-Sep-2021

[1]Área Curricular de Física, Departamento de Física, Universidad Nacional de Colombia, 11001, Bogotá D.C., Colombia.
[2]Grupo de Materiales Nanoestructurados y sus Aplicaciones, Departamento de Física, Universidad Nacional de Colombia, 11001, Bogotá D.C., Colombia.
[3]Grupo de Física de Nuevos Materiales, Departamento de Física, Universidad Nacional de Colombia, 11001, Bogotá D.C., Colombia.
Email: jroar@unal.edu.co

1 Introduction

Clay minerals are usually defined for being part of the phyllosilicates family, which are constituted by two layers, one of tetrahedral Silica and an octahedral coordinated sheet commonly composed by Mg, Al, K, Fe or Ca and O or OH [1], both of them are joined by apical oxygens or hydroxyls to form 1:1 (1 tetrahedral and 1 octahedral sheets a clay mineral layer) or 2:1 (2 tetrahedral and 1 octahedral between them forms a clay mineral layer) clays [2]. These have been widely used trough human history and represent an important field of research for industries such as pharmaceutical [3-5], construction [6-8], ceramics [9-11], etc.; not to mention that clay minerals are a constant subject of study for socio-cultural aspects of ancient civilizations [12-15] , emergence of life in earth [16-18] and some actual topics in investigation like water decontamination [19-21], chemical sensors [22-24], molecular sieves [25-26] etc. These characteristics make clay minerals research important beyond their geological concern on this topic, and hence physical properties of clay minerals such as crystalline structure, surface morphology, optical response, electrical measurements I(t), R(T) might be studied to obtain information on the applicability of each kind of clay [27-29]. It is important to note that the classification of clay minerals strongly depends on the subject area, here, tetrahedral-octahedral phyllosilicates are considered as clays, but the synthesis process ensures the common condition over the particle diameter (i.e., D $\leq$ 5 μm).

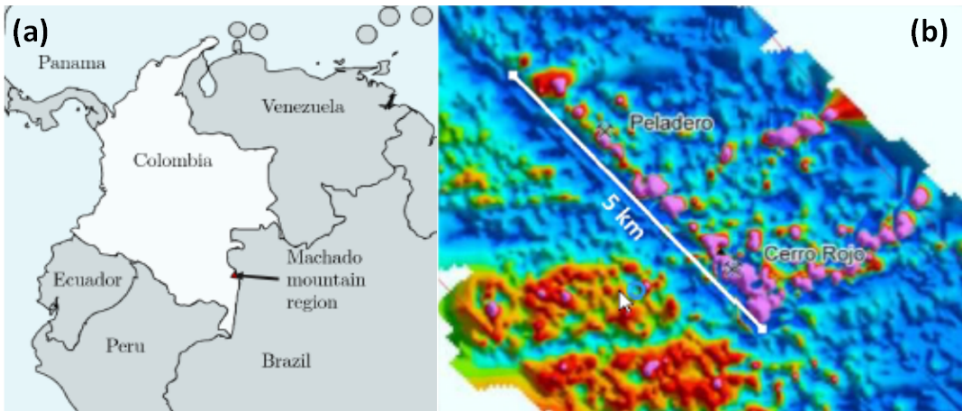

Figure 1. Geographic location of the provenance site of the studied clay.

In this work, the results of synthesis and physical characterization of a clay mineral from the Machado mountain region in the municipality of Tarairá, department of Vaupés, Colombia are reported. For this, X-Ray Diffraction (XRD), Scanning Electron Microscopy (SEM), Energy Dispersive X-Ray Spectroscopy (EDS), UV-Vis-NIR Spectroscopy, Current - time, Current- Voltage and Resistance - Temperature curves are applied in order to characterize the clay natural samples.

2 Experimental setup

In this section the experimental setups used to extract the clay from the rock are explained same as the synthesis of the clay samples and its characterization.

2.1 Sample provenance

The sample were obtained in the location of 'Cerro Rojo' in the Machado mountain range municipality of Tarairá, department of Vaupés, Colombia, showed in the map of figure 1) The zone present hilly relief and the rock was a part of an inactive gold mining work land with two sub-levels of approximately 100 m each, iron oxides and quartz outcrops were naked eye visible. Fragments of the rock were taken around a depth of h = 100 m from the entry.

2.2 Materials

The geological samples usually are formed by a lot of compounds with different grain sizes [31]. In order to separate the clay from the other constituents,

like sand, grave, silt, quartz, etc. The rock showed in figure 2.1 was macerated for two hours in an agate mortar (figure 2.2), after obtaining a homogeneous powder, it was sifted in a 400 mesh (i.e., a mesh size of 37 μm, see figure 2.3). In this step of the preparation process, it was expected to have a mixture of only carbonates, organics, silt, and clay (figure 2.4). The removal of carbonates is required in the limestones, in this case, it is not necessarily due to the geological origin of the rock [32-33]. The treatment to remove the organic part consists in a 3% solution bath of hydrogen peroxide (H_2O_2), nevertheless, before submerging all the sample it is advisable to do a test with a little powder fraction. If the organics removal is necessary, when the immerse into the solution is complete, one must observe bubbles in the surface of liquid. For the considered sample, the treatment is not necessary [34]. In this point, the sample powder is now only clay and slit. To separate these components is necessary to use a distilled water-powder solution with a mono-dispersant at 0.5% WW (figure 2.5)[35]. For this, sodium hexametaphosphate were used $(NaPO_3)_6$ in a highly diluted solution. After an 8-hour decanting process, the liquid and solid phases were separated using a pipette. In the liquid phase, the clay is suspended, and a different method is required for its extraction. Among the most used methods are decanting (2-3 weeks), evaporation in water bath and the centrifugation process. To avoid oxidation of the sample by the water bath or adding hydroxyls to the structure, it was decided to centrifuge the sample at 5000 rpm, achieving the clay extraction (figure 2.6). This new fine powder was left to dry in a desiccator with silica at 10 KPa.

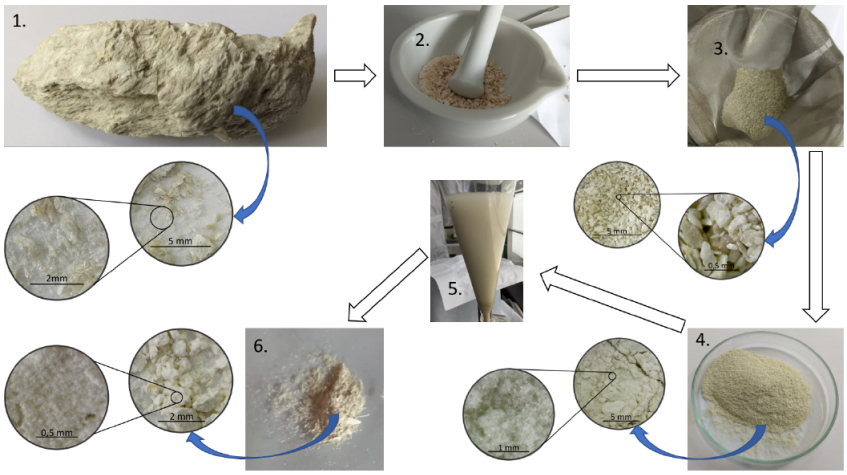

Figure 2. Schematic process of the most relevant steps for extract the clay to the rock. (1) Rock, (2) macerated rock, (3) sifted residue, (4) sifted powder, (5) distilled water-powder solution and (6) clay extracted. The insets in sub-figures 1, 3, 4 and 6 show zoom pictures to the corresponding materials.

2.3 Synthesis

Smear slides sample mounts were prepared to structural characterization [36] Heat treatments at various temperatures were applied in order to identify the clay minerals. The principal idea was to detect changes in the crystal structure spacings or loss in the structure. Depending on the temperature and mineral species, these treatments can collapse some peaks by dehydration or destroy of the crystal structures. However, it is necessary to remember that some of the changes caused by the heat treatments may be temporary, and that partial or complete rehydration may occur during cooling [37]. Annealing, in atmospheric pressure, at 673(4) K and 823(4) K, with a slowly cooled were performed for a posterior XRD analysis. Another characteristic of the families of clays is their behavior under ethylene glycol bath, which is used as an auxiliary treatment to expand swelling clays [38]. Two hours before the XRD measurement, a smear slide sample was impregnated with $C_2H_6O_2$ and left drying. In order to prepare the disks clay samples, the not-annealed centrifuged powder was pelletized to form disks of

9.00(2) mm diameter and 0,99(1) mm height in a hydraulic press of 0,47(3) GPa. Subsequently the discs were annealed at 873,15(4) K for 4 h, and slowly cooled until room temperature. Samples for electrical measurements were coated with silver conductive paint at 60% on both sides of the discs.

2.4 Characterization

The samples were characterized through XRD measurements by using X-ray diractometer X'Pert Pro polycrystal of PANalytical, equipped with a Cu-K source: 1.540598 Å, a difference of potential of 40 kV, current of 40 mA and a X'Celerator detector. The software used for comparison was X'Pert HighScore Plus, using Rietveld refinement. Morphological characterization of the samples was performed by a scanning electron microscope (SEM) Vega3 SB with tungsten source, a XFlash Detector 410M and an accelerating voltage of 10 kV under high vacuum conditions ($\sim 10^{-6}$ mbar) , also equipped with a SDD for EDXS measurements. Ten monolayers of AuPd were sputtered on the disc's surface to avoid the accumulation of charges in the surface. Optical properties of the samples were obtained using a monochromatic beam in an integrating sphere with a spectrophotometer reference Cary 5000 UV-VIS-NIR from Agilent at atmospheric pressure and room temperature. In the reflectance measurement was used a diffuse reflectance configuration with correction of baseline with BaSO4. The electrical measurements were realized using a four points configuration in an Electrometer 6517A of High Resistance Meter from KEITHLEY. Gold-plated silver electrodes were used, for measurements at room temperature those were arranged in a brass cage or in a cryostat for measurement with temperature variation. The temperature control in these characterizations was performed by a Cryogenic Temperature Controller Lake Shoree 332 with a PT100 as temperature sensor.

3 Results and discussion

3.1 Morphology

Scanning electron micrography of the clay disk sample was obtained for SE and BSE at a magnification of 6.27 kx, WD = 15 mm, and SEM HV = 15 kV. The obtained result can be seen in figure 3. The secondary electrons image (SE) of figure 3a show a non-planar surface topography probably caused in the pellet fabrication due to the observed platy morphology, while backscattered electrons image (BSE) of figure 3b did not show any relative difference in composition but rearms the previous observation of platy morphology in this sample. Meanwhile, a strong charging effect of the most superficial grains is observed due to the high potential difference applied to the electron gun of the microscope.

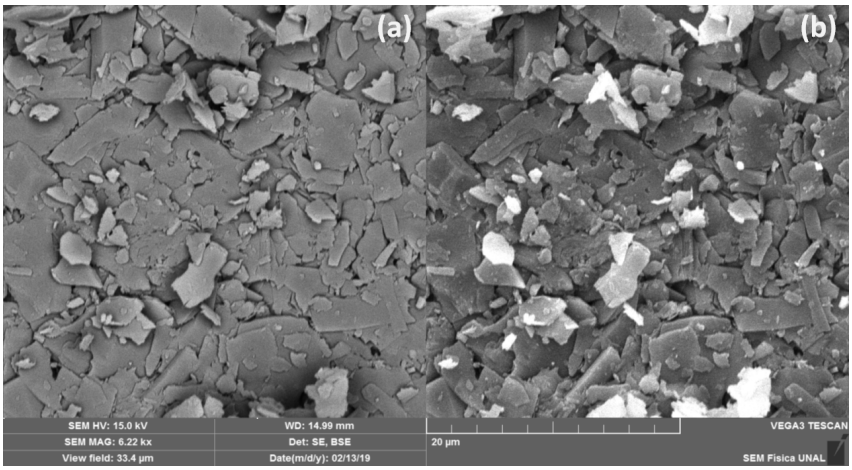

Figure 3. SE (a) and BSE (b) micrographs of clay disk showing platy morphology.

In order to obtain information on the mean grain size (area) the SE image was analyzed through particle area measurement analysis using the threshold value method to binarize the image after applying a FFT band-pass filter to enhance the contrast between the particles. Once the image was 8-bit threshold valued, an area measurement algorithm was used with minimum circularity parameter of 0.05. The obtained surface area data then pass to a histogram analysis that can be seen in figure 4, in which the inset reveals the contours used in the analysis.

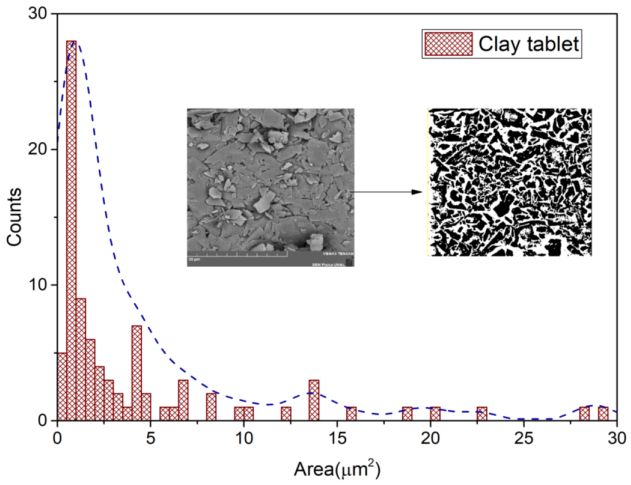

Figure 4. Histogram of area (red) and approximated distribution of grain size (blue).

p

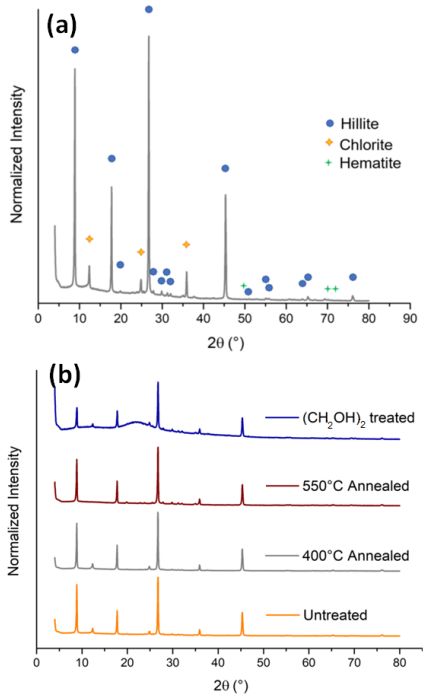

Figure 5. a) Identified peaks in the untreated sample and (b) series of XRD patterns to show Hillite and Chlorite presence in the sample.

Table 1. EDS analysis on the area represented in the micrograph of figure 3b.

Element	Atomic number	Atomic percent (%)	Deviation σ
O	8	48.00	2.45
Al	13	22.44	0.48
Si	14	22.12	0.44
K	19	6.84	0.17
Fe	26	0.60	0.07

This analysis allows to think that the average composition of the sample have significant oxygen in its structure, all the clay minerals include apical oxygens in the tetrahedral sheet, and central and extreme oxygens in the octahedral one, so that it's natural to think on high oxygen concentrations in the sample; The other elements present in the sample are common in nature and have been reported in the Mitú region plate near Tarairá, usually in phases of muscovite, chlorite, sericite, leucoxene and epidote [40], in this case, different clay minerals are expected based in the location of the sampling (an inactive gold mine).

3.3 Structure

Samples previously prepared as told in the 2.3 subsection were characterized following the Clay Mineral Identification Flow Diagram [41]. The four samples (Untreated, $C_2H_6O_2$ impregnated, 673 K and 823 K annealed) evidence the XRD patterns showed in figure 5a. The first two peaks in $2\theta = 8.85°$ and $2\theta = 12.3°$ equivalent to d-spacings of $d_1 = 10$ Å and $d_2 = 7$ Å were followed in the flow diagram. For d_1, the peak shows no changes over the treatments, which directly leads to the hillite, muscovite, glauconite, ceradonite and biotite family. Peaks at $d = 5$ Å and $d = 1.53$ Å allows to differ between the diverse clay minerals and choose the Hillite phase directly. As showed in figure 5b, for the second peak ($d_2 = 7$ Å), no changes were observed after $C_2H_6O_2$ impregnation, and 134 K anneal process, but total destruction is observed for the 823 K annealing, lead to the kaolinite, chlorite, dickite, nacrite families, as the observed morphology in the subsection 3.1. is platy, nacrite and dickite families are discarded, and then, by having a (060) diffraction peak around $d = 1.53$ Å, it is suggested the occurrence of chlorite over dioctahedral chlorite.

As seen in subsection 3.2 a small percentage of iron is present in the sample, usually magnetite [42-43], goethite or hematite[44] associated phases are present in clay minerals, Goethite-Hematite phases have been observed in the Mitú region and seems to be responsible of Oolitic iron presence in this region [39]. Then, a search-match algorithm for the present peaks in the untreated sample was used to see if the pattern is in accordance with the proposed crystallography, three phases from the COD 2013 database[45-49] were selected due to its accordance score. Hillite ($KA_{l4}Si_2O_{12}$) with PDF 96-900-966 [50], Chlorite ($Mg_3Si_2O_9$) with PDF 96-900-0159 [51] and Hematite (Fe_2O_3) with PDF 96-591-0083 [52]. The identified peaks are shown in figure 5a. Finally, Rietveld analysis was performed to determine the crystalline percentages in the present sample, obtaining a 96.3 % of Hillite phase, 1.7 % of Chlorite phase and a remaining 2.0 % of Hematite. The resulting structures are shown in figure 6.

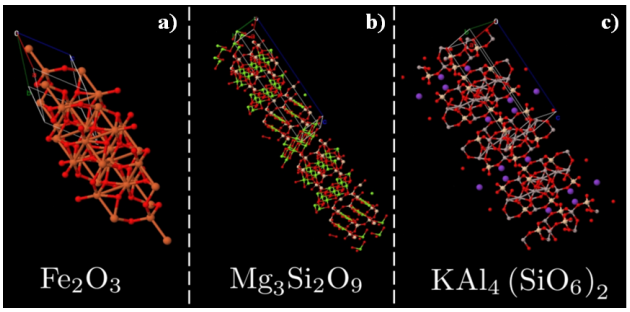

Figure 6. Rietveld solved structures for the three present phases in the sample. Primitive cell structures were solved with Materials project interface [53]

The solved structures show tetrahedral or octahedral coordinates cells. Observed Hematite (Fe_2O_3) has a Corundum-like structure and belongs to trigonal R-3c space group [54]. Trivalent iron (Fe^{3+}) is attached to six divalent oxygens (O^{2-}) forming a trigonal structure of sharing octahedra. For Chlorite ($Mg_3Si_2O_9$) we obtain triclinic P_1 space group with the expected three layers, one of $Mg_3Si_4O_{12}$, and other two of MgO_2 oriented in the hkl (001) direction. Two layers of SiO_4 tetrahedra shares apical oxygens with a MgO_6 octahedral sheet between them[51], forming a well-defined 2:1 clay mineral structure. In the other hand, Hillite ($KAl_4Si_2O_{12}$), that constitute the major component, crystallizes in monoclinic C2/c space group, analog to Chlorite. Hillite is a 2:1 clay mineral, with two layers of tetrahedral SiO_4/AlO_4 sandwich a layer of KO_6 octahedra, forming a non-uniform clay mineral layer due to the duality (Si, Al) in the tretrahedral layer [50].

3.4 Optical properties

The optical characterization was based on a diffuse reflectance spectroscopy (DRS) study. The sample was prepared in the form of a disk with a thickness of 0.99(1) mm and a diameter of 9.00(2) mm. The disk was placed in the center of a non-reflective black support within the UV-VIS-NIR integration sphere. Measurements were made in the range 200 nm $\leq \lambda \leq$ 1100 nm in steps of 1 nm. Even though the disk is so thick, the relative intensity of the reflected beam (figure 7a) is greater than 50% in the NIR-VIS spectrum, up to λ = 400 nm. The absorption coefficient was calculated considering a null-transmitted beam ($T = 0$) in the optical equations.

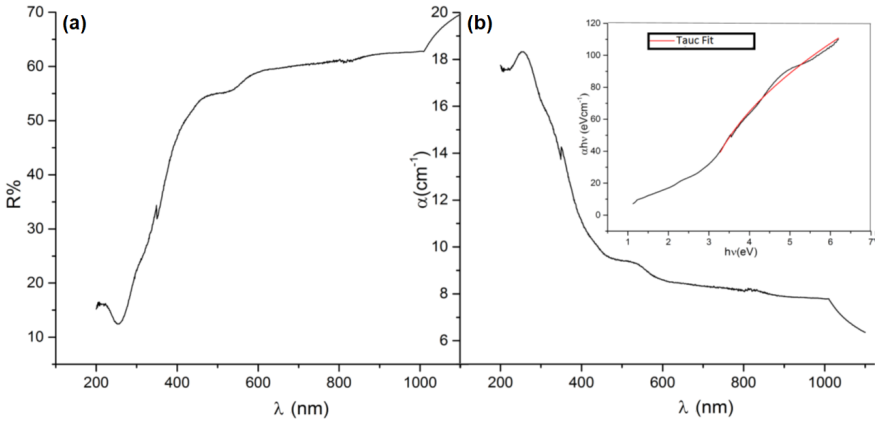

Figure 7. Optical properties as function of the wave longitude to the disk sample. (a) Diffuse reflectance in percentage, (b) absorption coefficient with a (inset) Tauc analysis.

The optical density (also known as absorption) is defined by

$$O.D = -log_{10}\left(\frac{I(l)}{I_o}\right), \tag{1}$$

where *I(l)* is the beam intensity at distance *l* and I_0 the initial intensity. Following the conservation principle, absorbed, transmitted, and reflected beams must comply

$$A + T + R = 1. \tag{2}$$

The absorption coefficient (α), in an optical medium is defined by [55]

$$dI(z) = -\alpha dz.I(z), \tag{3}$$

where the propagation direction is z, integrating the Beer-Lambert equation is deduced as

$$I(z) = I_o \exp(-\alpha z). \tag{4}$$

Combining Eq. 1 and Eq. 4, the relation between absorption and is found to be

$$O.D = \frac{\alpha l}{\ln(10)} \approx 0.434\alpha l. \tag{5}$$

The absorption coefficient was calculated from diffuse reflectance measurements (figure 7b), and a peak to absorption in UV range was found. This result means, possibly, in a photon absorption inside

the material in a particular wave longitude. Using the band gap concept of the semiconductors, the idea is to determine an effective band gap of the material by the Tauc method (see Jan Tauc [56]). The Method is mostly valid to semiconductors behaviors, and was refined by Davis and Mott [57, 58], leading to the following expression

$$(\alpha h\nu)^{\frac{1}{n}} = a(h\nu - E_g), \qquad (6)$$

where h is the Plank constant [59], ν is the photon incident frequency, α is the absorption coefficient, a represents a proportionality constant and E_g the band gap. The n factor depends on the nature of the transitions that govern mostly in the material. In general, n depends on if is a direct, indirect, allowed, and forbidden transition (see table 2). Using the Tauc analysis, the $\alpha h\nu$ as a function of $h\nu$ plotted in figure 7b allowed to a direct transition with E_g=*2.86 eV*, which corresponds to an electronic transition without phononic interactions that has place for a λ=*434 nm*.

Table 2. Possible values of n factor for Tauc analysis (Eq. 6) and it depend on the nature transition.

n	**Nature Transition**	
½	Direct	Allowed
3/2	Direct	Allowed
2	Indirect	Forbidden
3	Indirect	Forbidden

3.5 Electrical response

The circular faces of the samples were painted with silver dye for electrical characterization, so that each disk can be seen as a parallel plate capacitor, expecting an RC circuit behavior when subjected to a potential difference. A potential of 50 V was applied on the disk, and the behavior of the current over time was analyzed, as represented in figure 8. Initially a decreasing current is observed, but subsequently the current increases, reaching a stable current average value of *1.389(8) x* 10^{-7} *A*.

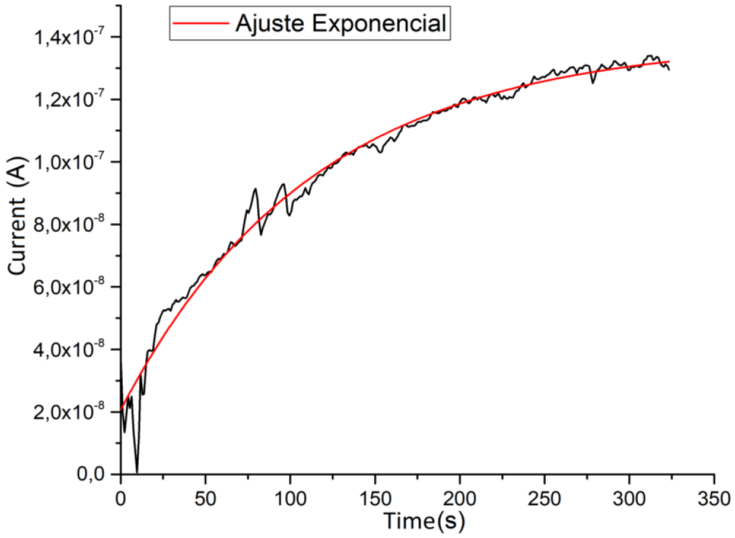

Figure 8. Current as function of time for a 50 Volt potential applied on the silver-painted sample.

The electrical response obtained follows a behavior given by the function

$$I(t) = \left[1.390 - 1.183e^{-\frac{t}{113}}\right] \text{x}10^{-7}\, A, \qquad (7)$$

which does not correspond to RC type behavior (which should not contain a temperature-independent term), due to the eventual occurrence of microscopic percolative processes that take place due to the random distribution of the three compounds that make up the clay mixture.

An interesting dependence is the resistive behavior as a function of temperature. Due to the ease with which clay absorbs water from the atmosphere, the electrical conductivity could increase due to

the distribution of hydrogen bonds in the material. Figure 9 depicts a heating up to $T = 350$ K, evidencing a decrease in resistance with temperature by an order of magnitude that clearly affects electrical losses.

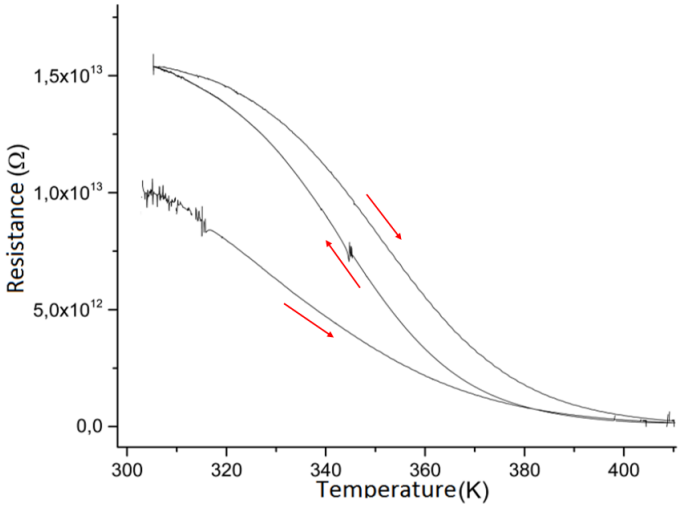

Figure 9. Current as function of time for a 50 Volt potential applied on the silver-painted sample.

The curve depicted in figure 9 shows a downward characteristic that varies with each measurement cycle due to the processes of absorption and evaporation of moisture from the environment. Meanwhile, in general, the order of magnitude of resistivity is typical of insulating type materials.

4 Conclusion

The proposed and used synthesis method economically, rapidly and affordably separates clay minerals from silt and sand. The size analysis by SEM shows that more than 99% of the observed sizes are in the region of clay diameter $D < 5$ µm. Morphological analysis helped to differentiate the illite phase from the muscovite, glauconite, cerandinite and biotite families, it also shows the characteristic lamellar structure of clay minerals due to the T-layer-O-layer-T-layer crystal structure. Thermal analysis and $C_2H_6O_2$ impregnation showed chlorite and illite phases, thanks to EDXS measurements also identified Fe_2O_3 phase with trigonal space group R-3c; both clay minerals in the structure showed tetragonal-octahedral-tetragonal 2:1 coordination with triclinic P1 and monoclinic C2/c space groups for chlorite and illite respectively. Due to the high reflectance in the infrared region, and its high absorption coefficient in the UV spectrum, the clay can be used as an environmentally friendly component of a sunscreen. Another particular optical property of this material is its insulating band gap. The electrical behavior of clay classifies this material in the insulating materials, and for the application of electrical shielding it is a very good coating for high voltage situations. The electrical properties have significant changes when the clay is in the presence of a humid climate, absorbing the surrounding water. This can be useful for a moisture sensor, or a moisture absorber. Due to the properties obtained, this material can be used to replace the old gold mining revenues in the 'Cerro Rojo' locality of the Machado mountainous region.

Acknowledgements

This work was partially supported by the Division of Investigation and Extension (DIEB) of the National University of Colombia.

References

[1] I. Bibi, J. Icenhower, N. Niazi, T. Naz, M. Shahid, S. Bashir, Clay minerals, in: Environmental Materials and Waste, Elsevier, pp. 543-567, 2016.

[2] H. H. Murray, Chapter 2 structure and composition of the clay minerals and their physical

and chemical properties, in: Developments in Clay Science, Elsevier, pp. 7-31, 2006.

[3] I. S. Khurana, S. Kaur, H. Kaur, R. K. Khurana, Multifaceted role of clay minerals in pharmaceuticals, *Future Science OA 1*, 2015.

[4] T. Thiebault, R. Guegan, M. Boussafir, Adsorption mechanisms of emerging micro-pollutants with a clay mineral: Case of tramadol and doxepine pharmaceutical products, *Journal of Colloid and Interface Science 453*, 1-8, 2015.

[5] M. Massaro, C. Colletti, G. Lazzara, S. Riela, The use of some clay minerals as natural resources for drug carrier applications, *Journal of Functional Biomaterials 9*, 58, 2018.

[6] D. Landinez, M. Calvo, C. Cárdenas, Caracterización de material arcilloso obtenido del rio Guaviare, vereda de La Paz, Colombia, Boletín de Ciencias de la Tierra 31-37, 2018.

[7] S. C. A. Mana, M.M. Hanafiah, A. J. K. Chowdhury, Environmental characteristics of clay and clay-basedminerals, 254 Geology, Ecology, and Landscapes 1, 155-161, 2017.

[8] A. Ariizumi, Clay in construction technology, *Journal of the Clay Science Society of Japan (in Japanese) 17* 256, 191-198, 1977.

[9] J. F. Burst, The application of clay minerals in ceramics, *Applied Clay Science 5*, 421-443, 1991.

[10] A. Bennour, S. Mahmoudi, E. Srasra, S. Boussen, N. Htira, Composition, firing behavior and ceramic properties 259 of the sejnene clays (northwest tunisia), *Applied Clay Science 115*, 30-38, 2015.

[11] O. M. Castellanos A., C. A. Rios R., M. A. Ramos G., E. V. Plaza P., A comparative study of mineralogical transformations in fired clays from the Valle Laboyos, Alto Magdalena basin (Colombia), *Boletin de Geología 34*, 43-55, 2012.

[12] J. Vukovic, Keramicke studije i arheometrija: izmeju analiza prirodnih nauka i arheoloske interpretacije, Issues in 264 *Ethnology and Anthropology 12*, 683, 2017.

[13] G. Rytwo, Clay minerals as an ancient nanotechnology: Historical uses of clay organic interactions, and future 266 possible perspectives, Macla: Revista de la Sociedad Española de Mineralogía, 2008.

[14] Z. L. E. Ntah, R. Sobott, B. Fabbri, K. Bente, Characterization of some archaeological ceramics and clay samples from Zamala - Far-northern part of Cameroon (West Central Africa), *Ceramica 63*, 413 - 422, 2017.

[15] M. A. Neupert, Clays of contention: An ethnoarchaeological study of factionalism and clay composition, *Journal of Archaeological Method and Theory 7*, 249-272, 2000.

[16] H. Hashizume, Role of clay minerals in chemical evolution and the origins of life, in: Clay Minerals in Nature - Their Characterization, Modification and Application, InTech, 2012, pp. 191-208.

[17] H. Hashizume, Adsorption of nucleic acid bases, ribose, and phosphate by some clay minerals, *Life 5*, 637-650, 2015.

[18] A. B. Subramaniam, J. Wan, A. Gopinath, H. A. Stone, Semi-permeable vesicles composed of natural clay, *Soft Matter 7*, 2600, 2011.

[19] H. Cripps, N. Isaias, A. Jowett, The use of clays as an aid to water purification, *Hydrometallurgy 1*, 373-387, 1976.

[20] F. Aziz, N. Ouazzani, L.Mandi,M.Muhammad, A. Uheida, Composite nanofibers of polyacrylonitrile/natural clay for decontamination of water containing pb(II), cu(II), zn(II) and pesticides, Separation Science and Technology 52, 58-70, 2016.

[21] E. Annan, B. Agyei-Tuour, Y. D. Bensah, D. S. Konadu, A. Yaya, B. Onwona-Agyeman, E. Nyankson, Application of clay ceramics and nanotechnology in water treatment: A review, *Cogent Engineering 5*, 1-35, 2018.

[22] U. Guth, S. Brosda, J. Schomburg, Applications of clay minerals in sensor techniques, *Applied Clay Science 11*, 229-236, 1996.

[23] H. L. Tcheumi, I. K. Tonle, A. Walcarius, E. Ngameni, Electrocatalytic and sensors properties of natural smectite type clay towards the detection of paraquat using a film-modified electrode, *American Journal of Analytical Chemistry 03*, 746-754, 2012.

[24] V. L. Reena, C. Pavithran, V. Verma, J. D. Sudha, Nanostructured multifunctional electromagnetic materials from the guest-host inorganic-organic hybrid ternary system of a polyaniline-clay-polyhydroxy iron composite: Preparation and properties, *The Journal of Physical Chemistry B 114*, 2578-2585, 2010.

[25] R.M. Barrer, Expanded clay minerals: a major class of molecular sieves, *Journal of Inclusion Phenomena 4*, 109-119, 1986.

[26] K. Abdmeziem-Hamoudi, B. Siert, Synthesis of molecular sieve zeolites from a smectite-type clay material, *Applied Clay Science 4*, 1-9, 1989.

[27] A. Pietrodangelo, R. Salzano, C. Bassani, S. Pareti, C. Perrino, Composition, size distribution, optical properties, and radiative effects of laboratory-resuspended pm10 from geological dust of the rome area, by electron microscopy and radiative transfer modelling, *Atmospheric Chemistry and Physics 15*, 13177-13194, 2015.

[28] L. S. Abdallah, A.M. Zihlif, Effect of grain size on the AC electrical properties of kaolinite/polystyrene composites, *Journal of Thermoplastic Composite Materials 23*, 779-792, 2010.

[29] A. Awwad, R. Ahmad, H. Alsyouri, Associated minerals and their influence on the optical properties of jordanian kaolin, *Jordan Journal of Earth and Environmental Sciences 2*, 66-71, 2009.

[30] C. resources Ltd, Exploring the Tarairá gold belt, 2014. https://www.cosigo.com/i/pdf/CorporatePresentation.pdf

[31] H. G. Dill, Residual clay deposits on basement rocks: The impact of climate and the geological setting on supergene argillitization in the bohemian massif, central Europe) and across the globe, Earth-Science Reviews 165, 1-58, 2017.

[32] D. Camuo, M. Del Monte, C. Sabbioni, Origin and growth mechanisms of the sulfated crusts on urban limestone, Water, Air, and Soil Pollution 19, 351-359, 1983.

[33] U. Coastal, M. G. program, A laboratory manual for x-ray powder diffraction: Acetic acid treatment to remove carbonates, https://pubs.usgs.gov/of/2001/of01-041/htmldocs/methods/acid.htm, 2001. Accessed: 2019-02-16.

[34] U. Coastal, M. G. program, A laboratory manual for x-ray powder diffraction: Removal of organic matter with hydrogen peroxide, https://pubs.usgs.gov/of/2001/of01-041/htmldocs/methods/h2o2.htm, 2001. Accessed: 2019-02-16.

[35] U. Coastal, M. G. program, A laboratory manual for x-ray powder diffraction: Separation of silt and clay by decantation for x-ray powder diffraction, https://pubs.usgs.gov/of/2001/of01-041/htmldocs/methods/decant.htm, 2001. Accessed: 2019-02-16.

[36] U. Coastal, M. G. program, A laboratory manual for x-ray powder diffraction: Smear slide sample mounts for x-ray powder diffraction, https://pubs.usgs.gov/of/2001/of01-041/htmldocs/methods/xsslide.htm, 2001. Accessed: 2019-02-16.

[37] U. Coastal, M. G. program, A laboratory manual for x-ray powder diffraction: Heat treatments for x-ray powder diffraction, https://pubs.usgs.gov/of/2001/of01-041/htmldocs/methods/heating.htm, 2001. Accessed: 2019-02-16.

[38] U. Coastal, M. G. program, A laboratory manual for x-ray powder diffraction: Ethylene glycol treatment, https://pubs.usgs.gov/of/2001/of01-041/htmldocs/methods/eglycol.htm, 2001. Accessed: 2019-02-16.

[39] G. Rodríguez, J. G. Bermúdez, C. Ramírez, K. Ramos, F. Ortiz, J. Sepúlveda, M. I. Sierra, hierro oolítico en el área del municipio de Mitú 327 (Departamento de Vaupés, Amazonía Colombiana), Boletín de Ciencias de la Tierra 25-33 (2013.

[40] G. García, J. Sepúlveda, C. Ramírez, F. Ortiz, K. Ramos, J. Bermúdez, M. Sierra-Rojas, Cartografía geológica y exploración geoquímica de la plancha 443 MIT, 2011.

[41] J. H. L.J. Poppe, V.F. Paskevich, D. Blackwood, A laboratory manual for x-ray powder diffraction, 2010. https://pubs.usgs.gov/of/2001/of01-041/index.htm.

[42] C. Galindo-Gonzalez, J. M. Feinberg, T. Kasama, L. C. Gontard, M. Posfai, I. Kosa, J. D. Duran, J. E. Gil, R. J. Harrison, R. E. Dunin-Borkowski, Magnetic and microscopic characterization of magnetite nanoparticles adhered to clay surfaces, *American Mineralogist 94*, 1120-1129, 2009.

[43] J. H. M. Viana, P. R. C. Couceiro, M. C. Pereira, J. D. Fabris, E. I. F. Filho, C. E. G. R. Schaefer, H. R. Rechenberg, W. A. P. Abrahao, E. C. Mantovani, Occurrence of magnetite in the sand fraction of an oxisol in the Brazilian savanna ecosystem, developed from a magnetite-free lithology, *Soil Research 44*, 71, 2006.

[44] U. Schwertmann, Goethite and hematite formation in the presence of clay minerals and gibbsite at 25c, Soil Science Society of America Journal 52, 288, 1988.

[45] A. Merkys, A. Vaitkus, J. Butkus, M. Okuli-Kazarinas, V. Kairys, S. Graulis, COD::CIF::Parser: an error correcting CIF parser for the Perl language, *Journal of Applied Crystallography 49*, 2016.

[46] S. Graulis, A. Merkys, A. Vaitkus, M. Okuli-Kazarinas, Computing stoichiometric molecular composition from 344 crystal structures, *Journal of Applied Crystallography 48*, 85-91, 2015.

[47] S. Graulis, A. Dakevi, A. Merkys, D. Chateigner, L. Lutterotti, M. Quirs, N. R. Serebryanaya, P. Moeck, R. T. Downs, A. Le Bail, Crystallography open database (cod): an open-access collection of crystal structures and platform for world-wide collaboration, *Nucleic Acids Research 40*, D420-D427, 2012.

[48] S. Grazulis, D. Chateigner, R. T. Downs, A. F. T. Yokochi, M. Quiros, L. Lutterotti, E. Manakova, J. Butkus, P. Moeck, A. Le Bail, Crystallography Open Database - an open-access collection of crystal structures, J*ournal of Applied Crystallography 42*,726-729, 2009.

[49] R. T. Downs, M. Hall-Wallace, The american mineralogist crystal structure database, A*merican Mineralogist 88*, 247-250, 2003.

[50] A. F. Gualtieri, Accuracy of XRPD QPA using the combined rietveld-RIR method, *Journal of Applied Crystallography 33*, 267-278, 2000.

[51] J. S. Lister, S. W. Bailey, Chlorite Polytypism: IV. Regular Two-Layer Structures, *American Mineralogist 52*, 1614-1631, 1967.

[52] L. W. Finger, R. M. Hazen, Crystal structure and isothermal compression of fe2o3, cr2o3, and v2o3 to 50 kbars, *Journal of Applied Physics 51*, 5362, 1980.

[53] A. Jain, S. P. Ong, G. Hautier,W. Chen,W. D. Richards, S. Dacek, S. Cholia, D. Gunter, D. Skinner, G. Ceder, K. A. Persson, The Materials Project: A materials genome approach to accelerating materials innovation, APL Materials 1, 011002, 2013.

[54] N. Pailhe, A. Wattiaux, M. Gaudon, A. Demourgues, Impact of structural features on pigment properties of alpha - fe2 o3 haematite,

Journal of Solid State Chemistry 181, 2697-2704, 2008.

[55] A. Fox, Optical Properties of Solids, Oxford master series in condensed matter physics, Oxford University Press, 2001.

[56] J. Tauc, R. Grigorovici, A. Vancu, Optical properties and electronic structure of amorphous germanium, Physica Status Solidi, b) 15, 627-637, 1966.

[57] E. A. Davis, N. F. Mott, Conduction in non-crystalline systems v. conductivity, optical absorption and photoconductivity in amorphous semiconductors, The Philosophical Magazine: A *Journal of Theoretical Experimental and Applied Physics 22*, 0903-0922, 1970.

[58] N. Mott, E. Davis, Electronic Processes in Non-Crystalline Materials, Electronic Processes in Non-crystalline Materials, OUP Oxford, 2012.

[59] Codata, Fundamental physical constants, 2019. http://physics.nist.gov/